Macromolecules

pubs.acs.org/Macromolecules
Article

Evaporation-Induced Self-Assembly of Diblock Copolymer Films in an Electric Field: A Simulation Study

Oliver Dreyer, Ludwig Schneider, Maryam Radjabian, Volker Abetz,* and Marcus Müller*

Cite This: *Macromolecules* 2023, 56, 6880−6890
Read Online

ABSTRACT: The self-assembly of cylinder-forming diblock copolymer solutions in the course of solvent evaporation in the presence of an electric field is studied by particle-based simulations. The electric field provides additional control of the evaporation-induced self-assembly (EISA) and enlarges the processing window, which results in the desired formation of cylindrical domains that are perpendicularly oriented to the film surface. Two effects of the electric field are highlighted: (i) If the components of the AB block copolymer exhibit different permittivities, dielectrophoretic forces align the internal AB interfaces along the electric field, rendering parallel cylinders unstable. (ii) If shallow density gradients in the course of EISA give rise to the unfavorable morphology of perpendicular cylinders and subjacent layers of spherical micelles, the application of an electric field results in an elongation of the cylindrical domains and suppresses sphere formation. The beneficial effect of an electric field can be rationalized by the layer evolution model (LEM), previously developed for EISA in the absence of an electric field.

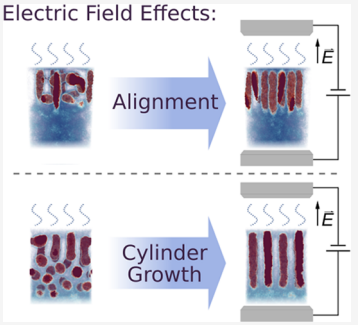

INTRODUCTION

Due to their ability to self-assemble into spatially modulated phases on the nanoscale,[1,2] block copolymers are considered promising materials for templating or fabricating dense, periodic nanostructures such as, *e.g.*, functional layers of nanoporous membranes.[3−9] Block copolymer materials form uniform structures with a low defect density and a periodicity on the nanoscale that can be precisely tailored by the molecular weight, capabilities that are difficult to achieve by other techniques on a large scale.

We focus on evaporation-induced self-assembly (EISA) in a film of cylinder-forming AB block copolymers. The diblock copolymer is dissolved, and the solution is subsequently cast to prepare a thin film, from which the solvent evaporates. Since the solvent mitigates the repulsive interactions between the polymer blocks, its evaporation increases the effective thermodynamic incompatibility, $\chi_{\mathrm{eff}}N$,[10−13] and induces microphase separation. The final self-assembled morphology depends on the processing conditions, and the kinetics of structure formation oftentimes lead to a metastable state rather than the thermodynamic equilibrium.[14−17]

How experimentally accessible, thermodynamic and process characteristics, such as, *e.g.*, solvent selectivity or rate of evaporation, influence the final morphology has been reported in previous experiments[18−20] and simulations.[21−24] For membrane applications, cylindrical domains oriented perpendicular to the film surface (*i.e.*, gas−liquid interface) are of particular interest and the crucial, aligning influence of the density gradient as a result of solvent evaporation has already been identified in previous experimental studies.[25−28] However, the understanding of the interplay between different fields—evaporation-induced density gradient and electric field—in the course of the dynamic ordering process remains a challenge.

Particle-based or field-theoretical simulations provide direct insights into the spatiotemporal evolution of different characteristics,[21−24] such as, *e.g.*, the three-dimensional morphology as a function of time and the statistics of single-molecule configurations, and allows the variation of parameters independently in order to elucidate their role. Simulations revealed the essential role of (i) solvent and vapor selectivity,[21,23,24] favoring the majority block, and (ii) fast evaporation rate.[21,22,24]

Recently, we have devised a layer evolution model (LEM)[24] to rationalize the influence of the different thermodynamic and processing parameters on the temporal evolution of the thickness of layers, l_{sph} and l_{cyl}, where spherical micelles initially form from a disordered copolymer−solvent mixture and where these micelles subsequently elongate to form the thermodynamically stable cylindrical morphology, respectively. The desired morphology of perpendicular cylinders forms if (i) both layers grow at similar speed and their spatial distance, $z_{\mathrm{b}} = l_{\mathrm{sph}} - l_{\mathrm{cyl}}$, remains smaller than the equilibrium thickness of a micelle layer or (ii) the growth rate of these layers surpasses

Received: June 22, 2023
Revised: August 8, 2023
Published: August 29, 2023

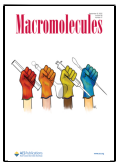

https://doi.org/10.1021/acs.macromol.3c01220
Macromolecules 2023, 56, 6880−6890

the induction time required to nucleate spherical micelles in the disordered polymer−solvent mixture.[24]

The present study expands on these conclusions by introducing an external electric field as an additional processing parameter. The dielectrophoretic aligning effect refers to the reduction of free energy by orienting AB interfaces between domains with different permittivity along the electric field vector.[29−48] Specifically, experimental work on membrane fabrication using EISA in electric fields reported two distinct effects:[49] A broadening of the experimental parameter window achieving the desired uniform, perpendicularly oriented morphology as well as longer cylindrical domains at the film surface.

In the present work, we investigate how an electric field influences the kinetics of structure formation and apply and generalize our LEM to rationalize the simulations. Our paper is arranged as follows: In the Model and Simulation Scheme section, we briefly describe the soft, highly coarse-grained, particle-based model and the implementation of the electric field that gives rise to the dielectric force, as well as detail the simulation setup. Subsequently, in the Results and Discussionsection, we discuss the alignment and accelerated growth of cylindrical domains induced by the electric field. The paper closes in the Conclusions section with a brief summary and outlook.

MODEL AND SIMULATION SCHEME

We consider a mixture of an asymmetric AB diblock copolymer, a solvent, S, and gas, G, in a thin film of volume, V.[24] Top and bottom (along the z-direction) of the simulation box are confined by impenetrable, nonselective walls. Periodic boundary conditions are applied along the two lateral directions, x and y. A sketch of the simulation setup is presented in Figure 1.

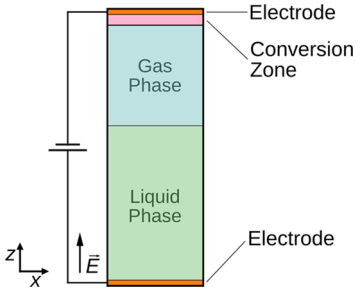

Figure 1. Sketch of the simulation box for the EISA simulations. The illustration shows the electrodes (orange) on top and bottom of the simulation box that additionally act as impenetrable walls. The conversion zone (pink) on top of the box is converting solvent to gas particles at regular intervals, mimicking the evaporation process.

In the highly coarse-grained model, particles interact via soft, pairwise potentials where the overall potential energy, $\mathcal{H}$, is divided into bonded, $\mathcal{H}_b$, and nonbonded contributions, $\mathcal{H}_{nb}$.

The strong, bonded interaction describes the connectivity along the polymer backbone of copolymers, which are discretized into $N_0 = 32$ particles and is represented by a harmonic potential.

$$\frac{\mathcal{H}_b}{k_B T} = \sum_m \sum_b \frac{3(N_0 - 1)}{2R_e^2}(\mathbf{r}_{m,b} - \mathbf{r}_{m,b+1})^2 \tag{1}$$

with k_B being the Boltzmann constant and T the temperature. R_e denotes the root-mean-square end-to-end distance of a polymer chain in the absence of nonbonded interactions; b enumerates the individual bonds; and $\mathbf{r}_{m,b}$ describes the position of the bth coarse-grained segment of molecule m. The finer the discretization, N_0, of the molecular contour, the larger the bonded forces between neighboring particles.

Solvent and gas molecules are represented by $N_S = N_G = 4$ particles. This fine discretization (i) couples neighboring grid cells because a molecule can straddle multiple cells and (ii) reduces the strength of nonbonded interactions per particle (*vide infra*).

The nonbonded contributions cater to short-range, pairwise interactions between all particles. They depend on the local, normalized densities of particles of type i

$$\hat{\phi}_i(\mathbf{r}) = \frac{1}{\rho_0}\sum_p \delta(\mathbf{r} - \mathbf{r}_p)\delta_{\mathrm{type}(p),i} \tag{2}$$

with ρ_0 referring to the average number density of particles, and the sum runs over all particles in the system. The Kronecker delta asserts that they are of type i. In accordance with our previous study,[24] we consider two compositions of the AB diblock copolymer, $f_A = \frac{N_A}{N_0} = \frac{9}{32}$ and $\frac{7}{32}$, respectively. In both cases, we observe the formation of cylinders of the minority component A. In the former case, we choose $L_x \times L_y \times L_z = 5 \times 5 \times 24.9\ R_e^3$, whereas in the latter case, we employ $5.8 \times 3.5 \times 49.9\ R_e^3$. Lengths L_x and L_y are selected to prevent structural frustration of the resulting morphology. For reasons explained later, simulations for the system featuring $f_A = \frac{7}{32}$ required a larger L_z which, in general, is computationally more costly, but this is compensated by a reduction of L_y.

The nonbonded interactions take the form

$$\frac{\mathcal{H}_{nb}}{k_B T\sqrt{\bar{N}}} = \int \frac{\mathrm{d}\mathbf{r}}{R_e^3}\left\{\frac{\kappa_0 N_0}{2}\left(\sum_i \hat{\phi}_i(\mathbf{r}) - 1\right)^2 + \sum_{i\neq j}\chi_{ij}N_0\hat{\phi}_i(\mathbf{r})\hat{\phi}_j(\mathbf{r})\right\} + \frac{\mathcal{H}_{el}}{k_B T\sqrt{\bar{N}}} \tag{3}$$

The first term restrains fluctuations of the local, normalized density, and the second term quantifies the pairwise repulsion between different molecules. κ_0 is proportional to the inverse isothermal compressibility, and χ_{ij} denotes the Flory−Huggins parameter between particles of species i and j, respectively. $\bar{N} = (\rho_0 R_e^3/N_0)^2 = 1000^2$ denotes the invariant degree of polymerization.

In the absence of explicit charges, the energy, $\mathcal{H}_{el}$, due to an electric field, $\mathbf{E} = -\nabla\psi$, depends on the local densities via the local permittivity ε

$$\mathcal{H}_{el} = -\frac{1}{2}\int \mathrm{d}\mathbf{r}\ \varepsilon(\{\hat{\phi}_i(\mathbf{r})\})|\nabla\psi(\mathbf{r})|^2 \tag{4}$$

where $\psi(\mathbf{r})$ denotes the electric potential. Introducing the typical scales of polymer systems, we rewrite eq 4 in the form

https://doi.org/10.1021/acs.macromol.3c01220
Macromolecules 2023, 56, 6880−6890

$$\frac{\mathcal{H}_{el}}{k_BT\sqrt{\bar{N}}} = -\frac{1}{2}\int \frac{d\mathbf{r}}{R_e^3}\frac{\varepsilon(\{\hat{\phi}_i(\mathbf{r})\})}{\varepsilon_0}\frac{\varepsilon_0 R_e}{k_BT\sqrt{\bar{N}}}|R_e\nabla\psi|^2$$
$$= -\frac{1}{2}\int \frac{d\mathbf{r}}{R_e^3}\frac{\varepsilon(\{\hat{\phi}_i(\mathbf{r})\})}{\varepsilon_0}|R_e\nabla\varphi|^2 \quad (5)$$

where we have defined the dimensionless electric potential

$$\varphi(\mathbf{r}) \equiv \psi(\mathbf{r})\sqrt{\frac{R_e\varepsilon_0}{k_BT\sqrt{\bar{N}}}} \quad (6)$$

By the same token, we measure the strength of the electric field in units of $\mathcal{E} \equiv \sqrt{\frac{k_BT\sqrt{\bar{N}}}{\varepsilon_0 R_e^3}}$.

In the following, we assume that the permittivity is the local density-weighted average and use the constitutive equation

$$\varepsilon(\{\hat{\phi}_i(\mathbf{r})\}) = \varepsilon_0\frac{\sum_i \varepsilon_i\hat{\phi}_i(\mathbf{r})}{\sum_i \hat{\phi}_i(\mathbf{r})} \quad (7)$$

where ε_0 stands for the vacuum permittivity and ε_i denotes the relative permittivity or dielectric constant of particle type i.

The electric potential is obtained by the Laplace equation

$$\nabla[\varepsilon(\{\hat{\phi}_i(\mathbf{r})\})\nabla\psi(\mathbf{r})] = 0 \quad (8)$$

Input values for the electrodes are chosen as $|\varphi| = 0$ for reference simulations without external electric field or in the range of $6.3 \le |\varphi| \le 7.9$, corresponding to an electric field of up to $E_0 = 0.06\,\mathcal{E}$, depending on system size. If systems exhibit regions with substantial density inhomogeneities, then the local field strength can vary.

In the following, we efficiently evaluate the densities and fields on a collocation grid. The normalized densities of particles of type i in grid cell, c, are defined as

$$\hat{\phi}_i(c) = \frac{1}{\rho_0\Delta L^3}\sum_p \Pi_c(\mathbf{r}_p)\delta_{\mathrm{type}(p),i} \quad (9)$$

with $\Delta L = R_e/10$ referring to the linear, spatial extent of a grid cell. The assignment function, Π_c, counts particles with position $\mathbf{r}_p$ within grid cell c. The bottom and top layers of the collocation grid accommodate the electrodes of the thin film and represent impenetrable walls for particles.

In order to exploit the scale separation between the strong bonded and weak nonbonded interactions, we employ the single-chain-in-mean-field (SCMF) algorithm.[50] To this end, the pairwise interactions are temporarily replaced by quasi-instantaneous fields, ω_i, that represent the nonbonded interaction of a particle of type i with its surrounding.

$$\frac{\omega_i(\mathbf{r})N_0}{k_BT} = \frac{R_e^3}{k_BT\sqrt{\bar{N}}}\frac{\delta\mathcal{H}_{nb}}{\delta\hat{\phi}_i(\mathbf{r})} \quad (10)$$

$$= \kappa_0 N_0\left(\sum_i \hat{\phi}_i(\mathbf{r}) - 1\right) + \sum_{i\neq j}\chi_{ij}N_0\hat{\phi}_j(\mathbf{r}) \quad (11)$$
$$- \frac{\sum_j(\varepsilon_i - \varepsilon_j)\hat{\phi}_j(\mathbf{r})}{2[\sum_j \hat{\phi}_j(\mathbf{r})]^2}|R_e\nabla\varphi|^2$$

(10)

These fields are computed from the instantaneous densities fields after every Monte Carlo step, and the quasi-instantaneous fields, ω_i, are updated accordingly. Between updates of the fields, the molecules evolve independently, and this additional layer of parallelism is efficiently employed in the graphics processing unit (GPU)-accelerated simulation program SOft coarse-grained MC Acceleration (SOMA).[51]

Trial displacements of particles are proposed by smart Monte Carlo (SMC) moves[52] that employ the strong bonded forces to bias the proposed displacement. Thus, the system features Rouse-like dynamics.[53] In one Monte Carlo (MC) step, each particle has the chance to be displaced once on average. We define the characteristic relaxation time, τ_R, as the time it takes the center of mass of a polymer to diffuse its own end-to-end distance, R_e, in a disordered system. $\tau_R \equiv R_e^2/D = 8130$ Monte Carlo steps (MCS), where D is the self-diffusion coefficient.

In order to solve Laplace's equation, eq 8, for the electric potential, φ, at every MCS, we use a Jacobi algorithm as relaxation method.[47,54] Densities, permittivity, and electric potential are defined on the collocation grid and a finite-difference stencil discretizes the gradients.[54,1] We found a sufficiently accurate minimization is achieved once $R_e\nabla\left[\frac{\varepsilon(\{\hat{\phi}_i(c)\})}{\varepsilon_0}R_e\nabla\varphi(c)\right] \le 10^{-2}/\sqrt[4]{\bar{N}}$ in every cell of the collocation grid.

Solving the electric potential during our evaporation simulations substantially increased the computation time up to a factor of 150. To accelerate the calculations for large simulation setups, we employed a simple convolution scheme. For this, a Gaussian smoothing kernel $g(\mathbf{r}) = \frac{1}{(2\pi\sigma^2)^{3/2}}\exp\left(-\frac{\mathbf{r}^2}{2\sigma^2}\right)$ with $\sigma = \Delta L$ and a cutoff of $3 \times 3 \times 3$ grid cells is used. The kernel smoothens the local permittivity on the collocation grid, and it skips every other cell in each dimension, resulting in a downsized (convoluted) grid that is 1/8 its original number of cells. Laplace's equation is solved as described above using the convoluted grid, which saves computational effort but makes a subsequent deconvolution necessary to transform the calculated electric potential back to the actual size of the collocation grid. This is achieved by weighing the values of the electric potential in each cell of the convoluted grid with each cell of the Gaussian kernel to restore the electric potential in the cells of the original collocation grid that formerly have been skipped. Since SOMA handles permittivity, electric potential, and density independently on the collocation grid, convolution of the local permittivity does not affect the local densities. Employing this scheme, simulations were faster by a factor of 30, *i.e.*, only 5 times slower compared to simulations with no electric field. Further discussion and illustration that convolution does not influence structure formation in the course of evaporation can be found in the Supporting Information.

To illustrate the aligning effect of the electric field and validate the implementation of the electric field in SOMA, we first consider a melt of symmetric diblock copolymers, $A_{16}B_{16}$. For this validation, the parameters differ from the EISA studies. We choose $\chi_{AB}N_0 = 15$ and $\kappa N_0 = 50$ and consider a simulation box of $16.8 \times 0.7 \times 8.4\ R_e^3$. The difference of the dimensionless electric potential, φ, between the electrodes was set to 6.3 which, together with $\varepsilon_A = 2$ and $\varepsilon_B = 8$, results in a strong electric field of approximately $E_0 \approx 0.13\,\mathcal{E}$.

Additionally, at $x = 0$ and $x = L_x = 16.8\ R_e$, one-cell-wide fields, covering the left and right sides of the simulation box,

https://doi.org/10.1021/acs.macromol.3c01220
Macromolecules 2023, 56, 6880−6890

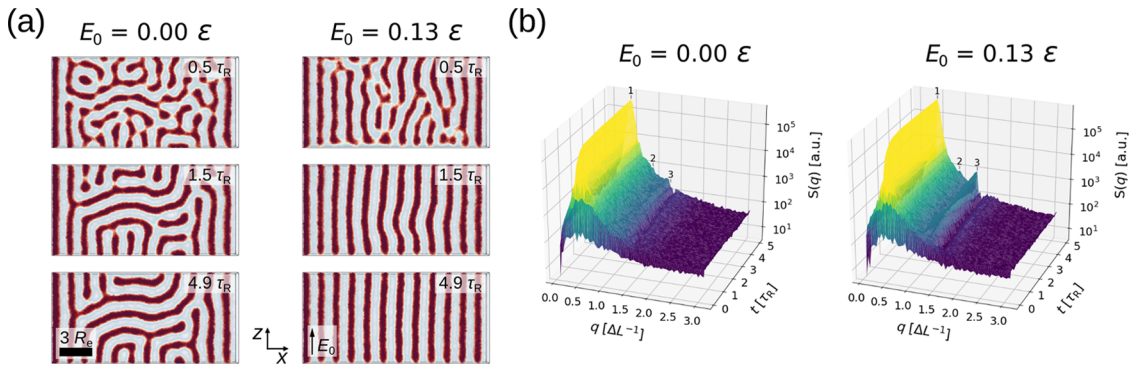

Figure 2. Comparison of melt simulations without ($E_0 = 0\,\mathcal{E}$) and with application of an electric field ($E_0 \approx 0.13\,\mathcal{E}$). (a) Density snapshots at selected simulation times, as indicated in the key. (b) Time evolution of the structure factor of $\phi_A - \phi_B$ fluctuations. Positions for the first three multiples of the peak positions (1, 2, and 3), indicating a lamellar structure, are marked in both plots, with $\Delta L = R_e/10$.

were implemented to effectively attract one component and guide the structure, *i.e.*, accelerate its alignment. The surface field at $x = 0$ is repulsive for B particles, $h_{0A}N_0 = 0$ and $h_{0B}N_0 = 10$. The opposite applies for the surface field at the right side, $x = 16.8\ R_e$, where $h_{xA}N_0 = 10$ and $h_{xB}N_0 = 0$.[47]

Figure 2a compares the ordering kinetics in a thin film with and without an electric field. In the latter case, the lamellae orientation still appears nonuniform, even for long times, 4.9 τ_R, after a quench from the disordered state, $\chi_{AB}N_0 = 0$. An electric field helps to align the domain interfaces along the direction of the field vector. This behavior was reported before.[29−48]

In addition, Figure 2b depicts the structure factor evolution of the density fields for both simulations. The first three peak positions of the typical peak sequence of a lamellar structure $\left(\frac{q_{lam}L_{lam}}{2\pi} = k = 1, 2, 3, \cdots\right)$,[55] with L_{lam} denoting the lamellar period, are marked. In the absence of an electric field, the lack of distinct peaks at the predetermined locations suggests a structure without long-range order. On the other hand, applying an electric field results in a peak at $q_{lam}R_e \approx 13.6 \approx 3{\cdot}4.5$, which starts forming around 0.5 τ_R and visibly grows until 3 τ_R. Afterward, the peak intensity increases only slightly. The fact that even peaks, *i.e.*, $k = 2$, are suppressed indicates highly symmetric phases, which is expected for a diblock copolymer with equal block size.[56]

We also note that the strength of the field cannot be increased arbitrarily. Too high values resulted in roughening of the film surface and a concomitant broadening of the film surface in the one-dimensional density profiles along the z axis (Figure S2a). We find that an upper limit of $E_0 \leq 0.06\,\mathcal{E}$ prevents these effects and is still strong enough to facilitate structure alignment in the course of EISA.

In the following study of EISA, we examine two different systems described by parameters similar to our previous study.[24] The model parameters are compiled in Table 1. Both systems yield minority block cylinders embedded in a majority block matrix, but the EISA processes differ. Systems with a polymer composition of A_9B_{23} are used to investigate the effect of an electric field on cylinder alignment, whereas a composition of A_7B_{25} is used to emphasize the increased cylinder growth rate.

Table 1. Compilation of the Model Parameters

polymer	$\chi_{AB}N_0$	$\chi_{AS}N_0$	$\chi_{BS}N_0$	$\chi_{AG}N_0$	$\chi_{BG}N_0$	κN_0	d_{vap} [R_e]
A_9B_{23}	95	20	0	75	75	150	static
A_7B_{25}	40	14	0	75	75	150	14.0

For all EISA studies, we use $\varepsilon_A = 2$ and $\varepsilon_B = 4$. These values are in the range of typical dielectric constants of polymers: polystyrene (PS): $\varepsilon = 2.5\ \varepsilon_0$, poly(methyl methacrylate) (PMMA): $\varepsilon = 3.7\ \varepsilon_0$, poly(2-vinylpyridine) (P2VP): $\varepsilon = 4.1\ \varepsilon_0$.[57,58] Solvent and gas permittivities are set to $\varepsilon_S = \varepsilon_G = 1$ in order to focus on the effect of the electric field on polymer morphology.

RESULTS AND DISCUSSION

In order to investigate the role of an external electric field on EISA, initially at $t = 0$, the simulation box includes AB diblock copolymer with an average, normalized number density, $\overline{\phi}_P = 0.25$, and solvent, but no gas. To effectively simulate evaporation, we employ a conversion zone at the upper boundary of the simulation cell, in which all solvent particles are converted to gas at an interval of 50 MCS. Similar approaches have been previously employed.[22−24,59] Alternatively, the conversion zone follows the established film surface at a constant distance, d_{vap}, increasing the evaporation rate at later times.

Two effects are studied in this work: (i) the facilitation of the formation of perpendicularly aligned cylinders of the minority block A, by an external electric field, and (ii) the increased growth rate of cylindrical domains. The results are compared to our previous study without external electric field[24] to highlight the aligning effect of the external electric field.

Previously, we described two main factors influencing the final orientation of the minority block cylinders, (i) surface selectivity of the diblock copolymer solution and (ii) evaporation rate, and introduced the layer evolution model (LEM) in order to rationalize our findings. These will be briefly summarized in the following, forming the basis to explain the influence of an external electric field:

First, it was observed that a thin surface layer of the minority block, in contact with the gas phase, is entropically favored and induces density oscillations in the homogeneous diblock copolymer solution beneath. This enrichment layer results in parallel cylinders in later stages. This behavior has been reported previously for diblock copolymer melts in contact with a chemically patterned surface, exhibiting an affinity for a certain block.[60,61] A solvent selective for the majority block helps to prevent the minority block surface layer and allows for

https://doi.org/10.1021/acs.macromol.3c01220
Macromolecules 2023, 56, 6880−6890

the formation of perpendicular cylinders. In this case, the solvent-swollen majority block displays an entropic preference comparable to that of the narrow surface of the polymer film for the minority block.

Additionally, the evaporation rate influences the resulting structure: Cylinders orient perpendicularly to the surface for higher rates and parallel for lower rates. To explain this, we introduced the layer evolution model (LEM), which features layers of thickness l_{sph} and l_{cyl}, in which minority blocks assemble into spheres and cylinders, respectively. During evaporation, a solvent-density gradient is created that reaches into the disordered diblock copolymer solution. At a certain point, the repulsive interaction of the different blocks of the copolymer is not sufficiently diluted by solvent, and microphase separation commences at the critical density of the order−disorder transition (ODT), $\phi_{P,ODT}$. The minority blocks initially assemble into A-spheres, embedded in a matrix of the majority block B. Depending on the magnitude of the solvent-density gradient, locally, the system may even cross the threshold density, $\phi_{P,OOT}$, for the order−order transition (OOT) from spherical micelles to cylindrical domains of the minority block. At the film surface, layers of thickness l_{sph} and l_{cyl} describe regions where the polymer density exceeds the threshold densities, $\rho_{P,ODT}$ or $\rho_{P,OOT}$, thereby enabling the formation of spheres or cylinders, respectively. The orientation of cylinders mainly depends on the growth rate of the layer, in which cylinders may form: Higher rates favor the alignment perpendicular to the film surface.

Cylinder Alignment by an Electric Field. First, the influence of an applied external electric field on the ODT and OOT densities was examined. Similar to our previous work,[24] bulk simulations of diblock copolymer solutions were used in order to obtain these values, and the results are shown in Table 2.

Table 2. Influence of the Electric Field on Order−Disorder (ODT) and Order−Order Transition (OOT) for a System with $\chi_{AB}N_0 = 95$ (See the Model and Simulation Scheme Section)

E_0 [$\mathcal{E}$]	ODT [ρ/ρ_0]	OOT [ρ/ρ_0]
0.00	0.30	0.42
0.03	0.29	0.39
0.06	0.29	0.32
0.13	0.29	0.32

Within the uncertainty, the electric field does not alter the ODT. Since our simulations are limited in the electric field strengths (see the Model and Simulation Schemesection), we cannot rule out that, besides $\rho_{P,OOT}$, extremely high values of E_0 also affect $\rho_{P,ODT}$. Former studies report a suppressive effect on density fluctuations due to an electric field, translating to an increase of $\rho_{P,ODT}$.[62,63] On the other hand, Amundson et al.[31] derived a function accounting for the change of the effective interaction parameter at the ODT of a copolymer, $\chi_{OD}N$, depending on the applied external electric field, which results in a decrease of $\rho_{P,ODT}$. Inserting typical values for the electric field strength of $E_0 = 0.06\,\mathcal{E}$ together with our definition $\mathcal{E} \equiv \sqrt{\frac{k_B T\sqrt{N}}{\varepsilon_0 R_e^3}}$ and a dielectric contrast $\Delta\varepsilon = 2$ yields a resulting, marginal change that agrees with our findings

$$\Delta\chi_{OD}N \sim 0.79\cdot\frac{\Delta\varepsilon^2\varepsilon_0}{k_B T\rho/N}E_0^2 = 0.79\cdot(\Delta\varepsilon\ 0.06)^2 \approx 0.01 \quad (12)$$

Additionally, a more complex constitutive equation for the permittivity, ε, that nonlinearly depends on the local polymer volume fraction gives rise to additional effects on the ODT.[64]

In contrast, the polymer density at the OOT, $\phi_{P,OOT}$, decreases with the strength of the electric field to 0.32 for $E_0 = 0.06\,\mathcal{E}$. This value is very close to the ODT, and a stronger field does not alter the OOT any further. Since the two blocks of the copolymer exhibit different permittivities, an electric field aligns the AB domain interfaces of the microphase-separated morphology in order to reduce the free energy of the system[29−48] (see also Figure 2). Thus, we attribute the OOT shift in the bulk mainly to the ellipsoidal distortion of the spherical domains in the electric field, favoring the transition to cylinders that are aligned along the electric field, which has been observed in previous studies.[38,65−67] Figure S3 in the Supporting Information features a bulk simulation of a similar diblock copolymer solution that exhibits a spherical morphology of the minority phase in the absence of an electric field. Upon an increase in the electric field strength, we observe that the spheres elongate until the formation of cylinders occurs. In our evaporation simulations, however, we do not observe a proper OOT from multiple vertically stacked layers of spheres to cylinders because the structure dynamically forms within an electric field as the solvent evaporates. The kinetics of structure formation will be discussed more thoroughly in a subsequent section.

As described in the Model and Simulation Schemesection, the electrodes in our simulations are positioned on top and bottom of the simulation box, creating an approximately homogeneous electric field perpendicular to the film surface. Accordingly, the chosen electrode geometry aims to favor the formation of perpendicularly aligned cylinders of the minority block during solvent evaporation.

Our dynamic solvent evaporation simulations exhibit only a small region close to the film surface, where microphase separation is possible. Here, mainly two factors impact the alignment of the minority block cylinders: (i) the solvent-density gradient, *e.g.*, controlled by the evaporation rate, that influences the emergence and growth rate of the thicknesses, l_{sph} and l_{cyl}, of spherical and cylindrical layers, respectively, and (ii) the absence or presence of a thin enrichment layer of the minority block at the film surface.[24] Thus, in order to align the cylinders along the electric field, the dielectrophoretic force must overcome the aforementioned effects, which can be achieved by increasing the electric field strength or the permittivity contrast between the blocks of the copolymer.

Solvent evaporation simulations with and without an applied external electric field are shown in Figure 3 for a diblock copolymer of the architecture A_9B_{23}. The remaining model parameters are presented in Table 1. Morphologies at different evaporation rates are depicted. The latter is controlled by the repulsion between solvent and gas, $\chi_{SG}N_0$, covering cases of fast ($\chi_{SG}N_0 = 0-10$) and slow evaporation ($\chi_{SG}N_0 = 30-40$), respectively. Since fast evaporation already yields perpendicularly aligned cylinders, additionally applying an electric field perpendicular to the film surface has no influence on alignment. However, as observed in the case of $\chi_{SG}N_0 = 0$, it facilitates the removal of defects.

https://doi.org/10.1021/acs.macromol.3c01220
Macromolecules 2023, 56, 6880−6890

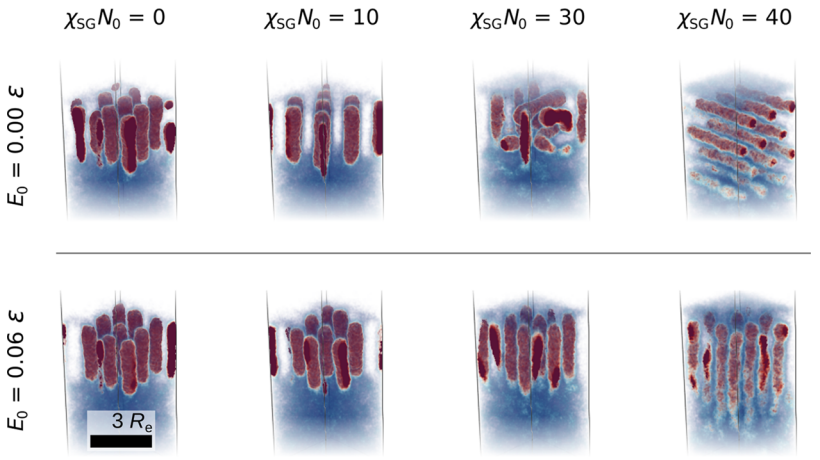

Figure 3. Influence of an external electric field on the final morphology for solvent evaporation simulations of fast, $\chi_{SG}N_0 = 0-10$ (at 17 τ_R and 21 τ_R, respectively), and slow evaporation rates, $\chi_{SG}N_0 = 30-40$ (at 60 τ_R and 112 τ_R, respectively). The top row depicts simulations in the absence of an electric field, $E_0 = 0$, whereas an electric field, $E_0 = 0.06\ \mathcal{E}$, was applied during solvent evaporation for simulations in the bottom row.

In the case of slow evaporation, l_{cyl} grows slower, and cylindrical domains may align parallel to the film surface. The transition from perpendicular to parallel cylinders gradually occurs with decreasing evaporation rate. At $\chi_{SG}N_0 = 30$, we observe a mixed cylinder orientation in the absence of an electric field, whereas parallel cylinders are exclusively observed at $\chi_{SG}N_0 = 40$. Applying $E_0 = 0.06\ \mathcal{E}$, however, yields solely perpendicular cylinders and shows that the dielectrophoretic force provides a dominant contribution to the alignment in these systems. Interestingly, for $\chi_{SG}N_0 = 40$ and $E_0 = 0.06\ \mathcal{E}$, cylinders appear slightly more irregular in shape compared to the other simulations, indicating the competition of the aforementioned aligning factors, *i.e.*, the contribution of the electric field to cylinder alignment is decreasing as the other factors gain importance. Nonetheless, similar to experimental work,[49] an electric field broadens the parameter window suitable for the perpendicular orientation of cylinders.

In order to understand how an electric field alters the mechanism of structure formation in the case of switching from parallel to perpendicular cylinder orientation, we focus on the early stages of microphase separation. Figure 4 compares the 1D density profiles of the minority block, A, at different electric field strengths. Without applying an electric field, a clear peak at $z = 11.2\ R_e$ is observed, which indicates the presence of a pronounced minority block layer at the film surface. Such a layer gives rise to composition oscillations in the solution and causes a parallel cylinder orientation.[24,61] In our electrode geometry, this minority block layer is perpendicular to the direction of the electric field, rendering its domain interface energetically unstable.[29−48] As expected, applying an electric field reduces the formation of the parallel surface layer, which can be inferred from the decreasing peak at $z = 11.2\ R_e$. The magnitude of this effect increases nonlinearly with the electric field strength, in qualitative agreement with the quadratic dependence of the dielectrophoretic force on the field strength, E_0.

The LEM highlights the kinetic nature of the aligning effect associated with the electric field. As shown in Table 2, an electric field shifts the OOT toward lower polymer densities so that ultimately both, ODT and OOT, occur within the same density range. Consequentially, the cylindrical layer thickness, l_{cyl}, grows faster than in the absence of an electric field and at a rate comparable to that of the spherical layer thickness, l_{sph}. This facilitates the formation of perpendicular cylinders.[24]

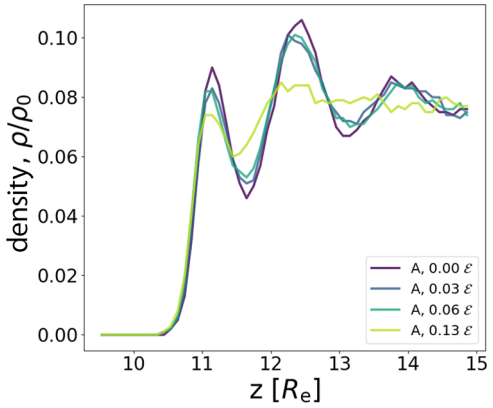

Figure 4. Influence of external electric fields on the minority block density close to the film surface for a system that features parallel cylinders, $\chi_{SG}\ N_0 = 40$. One-dimensional density profiles of the minority block, A, during structure formation at $t = 64\ \tau_R$, are shown as solid lines, where the color code refers to the applied electric field, $E_0 = 0 - 0.13\ \mathcal{E}$. ODT is crossed at 55 τ_R (in the absence of an electric field) and at 49 τ_R (with the application of an electric field). The film surface is located at $z = 10.8\ R_e$. The block−block interaction was set to $\chi_{AB}N_0 = 95$, and the remaining parameters are compiled in Table 1.

We emphasize that these two effects, dampening the composition oscillations (layering) at the film surface and an increased growth rate of l_{cyl}, enable perpendicular cylinders from the very beginning of phase separation. Accordingly, during solvent evaporation in an external electric field, no indication of morphological reorientation was found. We only observed the structure formation mechanism of the nucleation and growth of perpendicularly aligned cylinders. The next section will focus on the latter aspect.

Increased Cylinder Growth in an Electric Field. In addition to the alignment, experimental work also revealed that the application of an external electric field during solvent evaporation results in longer cylindrical microphases of the minority block.[49]

To highlight this effect in our simulations, we reduce the minority block fraction from $f_A = 0.28$ to $f_A = 0.22$ to shift the

https://doi.org/10.1021/acs.macromol.3c01220
Macromolecules 2023, 56, 6880−6890

morphology at the ODT more toward a spherical microstructure. Together with interaction parameters, $\chi_{AB}N_0 = 40$, $\chi_{AS}N_0 = 14$, and $\chi_{SG}N_0 = 0$, the simulation system has been studied in our earlier work (see Table 1 for a compilation of parameters).[24] Evaporation without an electric field yielded a final morphology of perpendicular cylinders with additional layers of spherical micelles beneath.

For such a system, an electric field of strength of 0.05 $\mathcal{E}$ shifts the polymer density at the ODT, $\rho_{P,ODT}$, from 0.70 to 0.69 and the polymer density at the OOT, $\rho_{P,OOT}$, from 0.82 to 0.77 in bulk simulations. Even though the difference from the OOT density is not as large as for the system presented in the previous section, the same trend is observed: Mainly the OOT is affected by the electric field, whereas the ODT remains virtually unaltered.

Thus, within the LEM, the application of an external electric field has no noticeable influence on the size of the spherical layer, l_{sph}, whereas the reduction of $\rho_{P,OOT}$ causes the cylindrical layer, l_{cyl}, to grow. Hence, in order to reveal the beneficial effect of an electric field, the system has to provide the possibility of a significant increase in l_{cyl}. Therefore, we chose a system with a shallow composition gradient. Then, in the absence of an electric field, the distance between the positions where the polymer density crosses the ODT and the OOT thresholds, $l_{sph}-l_{cyl}$, is large compared to a system with a steep composition gradient.

The system A_7B_{25} (Table 1) offers these advantages. The fact that layers of spheres emerge beneath perpendicularly oriented cylinders without electric field[24] signals a large spatial gap between the end of the regions where spheres and cylinders may form. Figure 5 highlights the growth of l_{cyl} in response to an electric field in a one-dimensional density profile at a time $t = 65\ \tau_R$. The upper panel serves as a reference, representing the system without application of an electric field, whereas the bottom panel presents the simulation with electric field applied. Layers where spheres or cylinders may form are indicated in green and red, respectively.

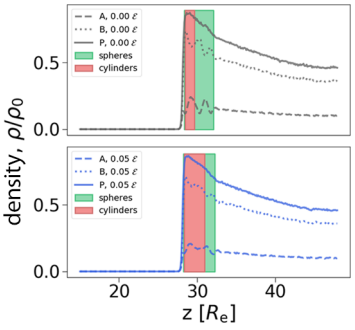

Figure 5. One-dimensional density profiles of solvent—evaporation simulations showing the effect of an electric field on the cylindrical layer, l_{cyl}, at $t = 65\ \tau_R$. Gray lines (top) represent the simulation without, and blue lines (bottom) with the application of an electric field, $E_0 = 0.05\ \mathcal{E}$. Solid, dashed, and dotted lines refer to minority block, A, majority block, B, and the sum of both, P, respectively. Spherical (green) and cylindrical layers (red) are highlighted in both panels.

The shallow polymer density gradient is clearly recognizable, extending deep into the copolymer solution. Please note that we increased the box length to $z = 49.9\ R_e$ to account for this fact. Comparing both plots, an electric field does not noticeably alter the shape of the overall polymer density profile (solid line). However, the electric field renders subjacent layers of spheres energetically unstable, due to the reduction of $\rho_{P,OOT}$, and causes a significant increase of the thickness, l_{cyl}, of the cylindrical layer, nearly doubling its size and enabling cylinder growth in a larger, deeper region of the film. This is additionally underlined by a distinct dampening of the composition oscillation.

A similar plot for a system featuring a configuration from the previous section, exhibiting exclusively perpendicular cylinders as well as a steep concentration gradient, contrasts how an electric-field-oriented orthogonal to the film surface is not able to visibly alter l_{cyl} under unfitting conditions and is presented in the Supporting Information (Figure S4).

Figure 6 displays the growth of the cylindrical layer, l_{cyl}, during solvent evaporation in system A_7B_{25} (a) without and (b) with the application of an electric field. The time-resolved layer evolution plots on the left help visualize how l_{cyl} distinctly changes, not only for a single time step, $t = 64\ \tau_R$ in Figure 5, but also during the entire course of the evaporation process. The reduction of $\rho_{P,OOT}$ in response to the electric field allows the emergence of a layer, in which cylinders may form, already at $t = 39\ \tau_R$, roughly 15 τ_R earlier than without the application of an electric field. Furthermore, an obvious increase in growth rate is observed where the difference between l_{cyl} and l_{sph} remains approximately constant, whereas in the absence of an electric field (top panel), this gap increases over time, expanding the region eligible for sphere formation. As a result, perpendicularly aligned cylinders are observed exclusively in the case of Figure 6b, leaving no space for subsequent layers of spheres, which would be energetically unfavorable anyway. The sequence of snapshots highlights that these cylinders do not originate from the connection of stacked layers of spheres but emerge entirely by continuous elongation of cylindrical domains perpendicular to the film surface—no OOT from multiple, vertically stacked layers of spheres to cylinders is observed; instead, the cylinders emerge from a single layer of spherical microdomains by gradual elongation in the course of solvent evaporation.

In addition, simulation snapshots in the absence of an electric field depict meandering cylinders (cf. Figure 6a), which are strongly fluctuating in the lower parts of the solution. In contrast, the application of an electric field during evaporation produces perfectly straight cylinders, emphasizing the aligning effect of the electric field.

To conclude, we would like to set these findings in the perspective of previous experimental studies. The results of this work display the general behavior that was observed in an experimental study of solvent evaporation from a diblock copolymer thin film in an external electric field.[49] Since it is difficult to follow the mechanisms in such experiments *in situ*, the longer cylindrical microstructure of the final membrane could only be explained qualitatively. For this, the theoretical work of Phillip et al.[18] was considered, arguing that the cylinder orientation tends to transition toward parallel alignment in deeper regions of the solution due to the velocity decrease of the ordering front. It was assumed that an electric field renders the parallel alignment in the lower parts of the cylinders energetically unstable and consequently increases the window of process parameters appropriate for perpendicular cylinder orientation.

Indeed, our simulations reveal a similar behavior, indicated by the expansion of l_{cyl}, although no cylindrical morphology was observed that exhibited both perpendicular and parallel

https://doi.org/10.1021/acs.macromol.3c01220
Macromolecules 2023, 56, 6880−6890

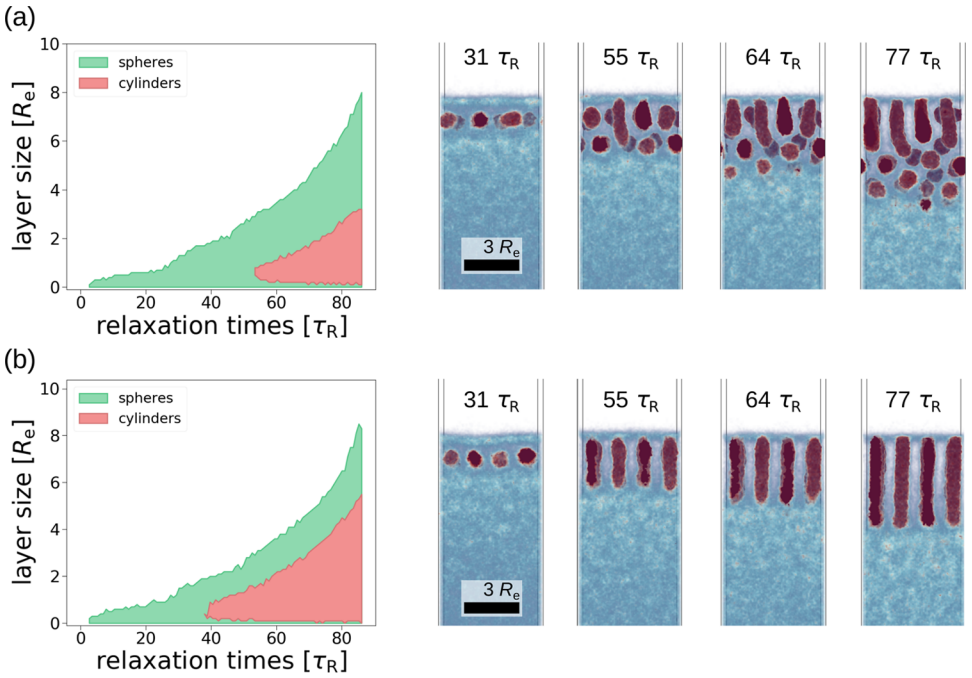

Figure 6. Solvent evaporation simulation (a) without and (b) with the application of an electric field of $E_0 = 0.05\ \mathcal{E}$. Left plots depict the growth of the spherical (green) and cylindrical layers (red), l_{sph} and l_{cyl}, respectively. Here, the absolute positions of the individual layers within the liquid phase are measured with respect to the gas−liquid interface at $z = 0$. Additionally, snapshots of the minority block density at given time steps are presented.

alignment depending on position. Here, the beneficial effect of an electric field does not originate from the energetic instability of parallel cylinders but from the instability of spherical micelles in the presence of an electric field.[38] The findings suggest that the effect is most pronounced in solutions that, in the absence of an electric field, exhibit a considerable difference between $\rho_{P,ODT}$ and $\rho_{P,OOT}$ and, as a consequence, form layers of spherical micelles subjacent to perpendicularly aligned cylinders during solvent evaporation.

Furthermore, simulations highlight that the structure dynamically forms as the solvent evaporates and that the kinetic effects due to an electric field, *i.e.*, domain alignment along its direction, causes continuous growth of cylinders exclusively without any sign of reorientation mechanism observed for cylindrical structures in bulk systems.[37]

Accordingly, we expect a similar morphology in experiments. In fact, previous work already observed that diblock copolymer casting solutions, depending on solvent properties, may exhibit micelle formation.[20,68−70] This indicates that the whole solution is close to or beyond the ODT. The latter case gives rise to a considerable layer of spherical micelles even before solvent evaporation. Applying an electric field would result in a substantial increase of l_{cyl} for the reasons given above, supporting the findings of this study.

Besides an increase in cylinder length, an electric field only has a minor effect on a system exhibiting the desired morphology of perpendicularly aligned cylinders. Since the internal AB interfaces are aligned parallel to the electric field, the morphology already minimized the electrostatic contribution to the free energy. However, deviating from near-perfect simulation parameters, resulting in parallel or ill-aligned cylinders, emphasizes the realigning effect of the electric field, which broadens the suitable parameter window and its ability to compensate unfitting conditions.

CONCLUSIONS

By implementing an external electric field into the soft, coarse-grained particle and the GPU-accelerated simulation program SOMA, we were able to study its influence on structure formation in a diblock copolymer solution during solvent evaporation. In our previous work, we have introduced the layer evolution model (LEM), aiming to explain how the morphology forms during solvent evaporation, depending on the evolution of layers with thicknesses, l_{sph} or l_{sph}, appropriate for sphere or cylinder formation, respectively. This concept proved also useful in the present study to analyze the structure formation under the influence of an external electric field.

Here, we focused on simulation systems where the evaporation of a solvent from a diblock copolymer solution yields a morphology consisting of cylindrical domains of the minority block, embedded in a majority block matrix. In order to respond to an electric field, the two blocks exhibit different permittivities. Plate electrodes were employed on the top and bottom of the simulation box, additionally acting as impenetrable walls for particles. The resulting, approximately homogeneous electric field is directed perpendicular to the film surface in such a way that it supports the desired structure, *i.e.*, perpendicular cylinders. Two particular effects are highlighted, which have previously been reported in experimental work:[49] Cylinder alignment parallel to the electric field vector as well as an increased growth rate and length of the cylindrical domains due to the electric field.

As a result of their permittivity difference, the dielectrophoretic force orients the domain interfaces along the electric field to reduce the electrostatic energy of the system. In addition to the resulting kinetic effects, simulations revealed mainly one further aligning contributor: In systems producing parallel cylinder orientation, *e.g.*, due to lower evaporation rates, the minority block forms a thin surface layer, which induces

https://doi.org/10.1021/acs.macromol.3c01220
Macromolecules 2023, 56, 6880−6890

density oscillations yielding parallel alignment in later stages. In our electrode geometry, such a layer is orthogonal to the electric field and therefore suppressed, facilitating perpendicular cylinder formation.

Furthermore, an electric field renders the spherical microstructures of the minority block energetically unstable and, as a result, reduces the polymer density for the order−order transition (OOT) from spherical to cylindrical microdomains, $\rho_{P,OOT}$, which, under judiciously chosen conditions, allows for a substantial increase in l_{cyl} and, thus, longer cylinders. However, since the order−disorder transition (ODT) density, $\rho_{P,ODT}$, is hardly affected by the electric field, a suitable system needs to exhibit a large spatial distance between the end of the cylinder and sphere-forming layers to enable such expansion. We found that systems featuring a shallow solvent gradient, reaching deep into the solution, are most convenient and represent a final morphology of perpendicular cylinder and subjacent layers of spheres. An electric field is able to increase l_{cyl} almost to the size of l_{sph} so that sphere formation is strongly suppressed, and solely cylinders nucleate and grow perpendicular to the film surface in the course of evaporation-induced self-assembly (EISA). We would like to note that during our simulations with electric field, we exclusively observed continuous cylinder growth without merging of spheres. Since experimental work on membrane fabrication observed the same general effects of an external electric field, these findings indicate a good agreement between this study and experiments.

Our simulations provided direct insights into the underlying mechanisms responsible for the controlled evolution of perpendicularly aligned cylinders during the solvent evaporation step in casting block copolymer membranes. Combining these findings with studies of non-solvent-induced phase separation (NIPS)[59] will provide an opportunity to map out the window of thermodynamic and processing parameters that allow for the formation of integral asymmetric membranes.[8,9]

■ ASSOCIATED CONTENT

Supporting Information

The Supporting Information is available free of charge at https://pubs.acs.org/doi/10.1021/acs.macromol.3c01220.

Additional experimental details and simulation results including supplemental figures, graphs, and discussions (PDF)

■ AUTHOR INFORMATION

Corresponding Authors

Volker Abetz − *Institut für Membranforschung, Helmholtz-Zentrum Hereon, 21502 Geesthacht, Germany; Institut für Physikalische Chemie, Universität Hamburg, 20146 Hamburg, Germany;* orcid.org/0000-0002-4840-6611; Email: volker.abetz@hereon.de

Marcus Müller − *Georg-August Universität Göttingen, Institut für Theoretische Physik, 37077 Göttingen, Germany;* orcid.org/0000-0002-7472-973X; Email: mmueller@theorie.physik.uni-goettingen.de

Authors

Oliver Dreyer − *Institut für Membranforschung, Helmholtz-Zentrum Hereon, 21502 Geesthacht, Germany;* orcid.org/0000-0003-0043-9489

Ludwig Schneider − *Georg-August Universität Göttingen, Institut für Theoretische Physik, 37077 Göttingen, Germany; Pritzker School of Molecular Engineering, University of Chicago, Chicago, Illinois 60637, United States;* orcid.org/0000-0002-3910-8217

Maryam Radjabian − *Institut für Membranforschung, Helmholtz-Zentrum Hereon, 21502 Geesthacht, Germany;* orcid.org/0000-0001-6869-4270

Complete contact information is available at: https://pubs.acs.org/10.1021/acs.macromol.3c01220

Notes

The authors declare no competing financial interest.

■ ACKNOWLEDGMENTS

Financial support was provided by the I2B project DIGIZWIMEM by Helmholtz-Zentrum Hereon, the Bundesministerium für Bildung und Forschung (BMBF) within the project 16ME0658K MExMeMo, and the Deutsche Forschungsgemeinschaft (DFG) under grant Mu1674/18-1. L.S. is grateful for the support of the Eric and Wendy Schmidt AI in Science Postdoctoral Fellowship at the University of Chicago. The authors gratefully acknowledge the Gauss Centre for Supercomputing e.V. (www.gauss-centre.eu) for providing computing time through the John von Neumann Institute for Computing (NIC) on the GCS Supercomputer JUWELS at Jülich Supercomputing Centre (JSC) and the HPC "Strand" of Hereon.

■ ADDITIONAL NOTE

[1]We illustrate the discretization of eq 8 for a one-dimensional collocation grid; the generalization to a three-dimensional grid is straightforward. Let $c\Delta L$ denote the position of grid cell c, then the discretized Laplace equation takes the form

$$\begin{aligned} 0 &= \left[\left(\varepsilon(c) + \frac{\varepsilon(c+1)-\varepsilon(c-1)}{2\Delta L}\frac{\Delta L}{2}\right)\frac{\varphi(c+1)-\varphi(c)}{\Delta L}\right. \\ &\quad \left. - \left(\varepsilon(c) - \frac{\varepsilon(c+1)-\varepsilon(c-1)}{2\Delta L}\frac{\Delta L}{2}\right)\frac{\varphi(c)-\varphi(c-1)}{\Delta L}\right]/\Delta L \\ &= \left[\left(\varepsilon(c) + \frac{\varepsilon(c+1)-\varepsilon(c-1)}{4}\right)\varphi(c+1) - 2\varepsilon(c)\varphi(c)\right. \\ &\quad \left. + \left(\varepsilon(c) - \frac{\varepsilon(c+1)-\varepsilon(c-1)}{4}\right)\varphi(c-1)\right]/\Delta L^2 \end{aligned}$$

Rearrangement yields

$$\begin{aligned} \varphi(c) = &\left[\left(\varepsilon(c) + \frac{\varepsilon(c+1)-\varepsilon(c-1)}{4}\right)\varphi(c+1)\right. \\ &\left. + \left(\varepsilon(c) - \frac{\varepsilon(c+1)-\varepsilon(c-1)}{4}\right)\varphi(c-1)\right]/[2\varepsilon(c)] \end{aligned}$$

which is solved by iteration.

■ REFERENCES

(1) Leibler, L. Theory of Microphase Separation in Block Copolymers. *Macromolecules* **1980**, *13*, 1602−1617.

(2) Bates, C. M.; Bates, F. S. 50th Anniversary Perspective: Block Polymers-Pure Potential. *Macromolecules* **2017**, *50*, 3−22.

(3) Polarz, S.; Antonietti, M. Porous materials via nanocasting procedures: innovative materials and learning about soft-matter organization. *Chem. Commun.* **2002**, *22*, 2593−2604.

(4) Takekoh, R.; Russel, T. P. Multi-Length Scale Porous Polymers. *Adv. Funct. Mater.* **2014**, *24*, 1483−1489.

(5) Dorin, R. M.; Sai, H.; Wiesner, U. Hierarchically Porous Materials from Block Copolymers. *Chem. Mater.* **2014**, *26*, 339−347.

(6) Abetz, V. Isoporous Block Copolymer Membranes. *Macromol. Rapid Commun.* **2015**, *36*, 10−22.
(7) Zhang, Y.; Mulvenna, R. A.; Qu, S.; Boudouris, B. W.; Phillip, W. A. Block Polymer Membranes Functionalized with Nanoconfined Polyelectrolyte Brushes Achieve Sub-Nanometer Selectivity. *ACS Macro Lett.* **2017**, *6*, 726−732.
(8) Radjabian, M.; Abetz, V. Advanced porous polymer membranes from self-assembling block copolymers. *Prog. Polym. Sci.* **2020**, *102*, 101219.
(9) Müller, M.; Abetz, V. Nonequilibrium Processes in Polymer Membrane Formation: Theory and Experiment. *Chem. Rev.* **2021**, *121*, 14189−14231.
(10) Joanny, J. F.; Leibler, L.; Ball, R. Is Chemical Mismatch Important in Polymer-Solutions. *J. Chem. Phys.* **1984**, *81*, 4640−4656.
(11) Schäfer, L.; Kappeler, C. A renormalization-group analysis of ternary polymer-solutions. *J. Phys.* **1985**, *46*, 1853.
(12) Olvera de la Cruz, M. Theory of microphase separation in block copolymer solutions. *J. Chem. Phys.* **1989**, *90*, 1995−2002.
(13) Müller, M.; Binder, K.; Schäfer, L. Intra- and Interchain Correlations in Semidilute Polymer Solutions: Monte Carlo Simulations and Renormalization Group Results. *Macromolecules* **2000**, *33*, 4568−4580.
(14) Zhang, C.-Z.; Wang, Z.-G. Random Isotropic Structures and Possible Glass Transitions in Diblock Copolymer Melts. *Phys. Rev. E* **2006**, *73*, 031804.
(15) Ren, Y.; Müller, M. Kinetics of pattern formation in symmetric diblock copolymer melts. **2018**, *148*. 204908. .
(16) Abetz, V.; Kremer, K.; Müller, M.; Reiter, G. Functional Macromolecular Systems: Kinetic Pathways to Obtain Tailored Structures. *Macromol. Chem. Phys.* **2019**, *220*, No. 1800334.
(17) Müller, M. Process-directed self-assembly of copolymers: Results of and challenges for simulation studies. *Prog. Polym. Sci.* **2020**, *101*, No. 101198.
(18) Phillip, W. A.; Hillmyer, M. A.; Cussler, E. L. Cylinder Orientation Mechanism in Block Copolymer Thin Films Upon Solvent Evaporation. *Macromolecules* **2010**, *43*, 7763−7770.
(19) Sutisna, B.; Polymeropoulos, G.; Musteata, V.; Peinemann, K.-V.; Avgeropoulos, A.; Smilgies, D.-M.; Hadjichristidis, N.; Nunes, S. P. Design of block copolymer membranes using segregation strength trend lines. *Mol. Syst. Des. Eng.* **2016**, *1*, 278−289.
(20) Radjabian, M.; Abetz, C.; Fischer, B.; Meyer, A.; Abetz, V. Influence of Solvent on the Structure of an Amphiphilic Block Copolymer in Solution and in Formation of an Integral Asymmetric Membrane. *ACS Appl. Mater. Interfaces* **2017**, *9*, 31224−31234.
(21) Paradiso, S. P.; Delaney, K. T.; García-Cervera, C. J.; Ceniceros, H. D.; Fredrickson, G. H. Block copolymer Self Assembly during Rapid Solvent Evaporation: Insights into Cylinder Growth and Stability. *ACS Macro Lett.* **2014**, *3*, 16−20.
(22) Berezkin, A. V.; Papadakis, C. M.; Potemkin, I. I. Vertical Domain Orientation in Cylinder-Forming Diblock Copolymer Films upon Solvent Vapor Annealing. *Macromolecules* **2016**, *49*, 415−424.
(23) Hao, J.; Wang, Z.; Wang, Z.; Yin, Y.; Jiang, R.; Li, B.; Wang, Q. Self-Assembly in Block Copolymer Thin Films upon Solvent Evaporation: A Simulation Study. *Macromolecules* **2017**, *50*, 4384−4396.
(24) Dreyer, O.; Ibbeken, G.; Schneider, L.; Blagojevic, N.; Radjabian, M.; Abetz, V.; Müller, M. Simulation of Solvent Evaporation from a Diblock Copolymer Film: Orientation of the Cylindrical Mesophase. *Macromolecules* **2022**, *55*, 7564−7582.
(25) Peinemann, K.-V.; Abetz, V.; Simon, P. F. W. Asymmetric superstructure formed in a block copolymer via phase separation. *Nat. Mater.* **2007**, *6*, 992−996.
(26) Kim, S. H.; Misner, M. J.; Xu, T.; Kimura, M.; Russell, T. P. Highly Oriented and Ordered Arrays from Block Copolymers via Solvent Evaporation. *Adv. Mater.* **2004**, *16*, 226−231.
(27) Jung, A.; Rangou, S.; Abetz, C.; Filiz, V.; Abetz, V. Structure Formation of Integral Asymmetric Composite Membranes of Polystyrene-block- Poly(2-vinylpyridine) on a Nonwoven. *Macromol. Mater. Eng.* **2012**, *297*, 790−798.
(28) Rangou, S.; Buhr, K.; Filiz, V.; Clodt, J. I.; Lademann, B.; Hahn, J.; Jung, A.; Abetz, V. Self-organized isoporous membranes with tailored pore sizes. *J. Membr. Sci.* **2014**, *451*, 266−275.
(29) Amundson, K.; Helfand, E.; Davis, D. D.; Quan, X.; Patel, S. S.; Smith, S. D. Effect of an Electric Field on Block Copolymer Microstructure. *Macromolecules* **1991**, *24*, 6546−6548.
(30) Amundson, K.; Helfand, E.; Quan, X.; Smith, S. D. Alignment of lamellar block copolymer microstructure in an electric field. 1. Alignment kinetics. *Macromolecules* **1993**, *26*, 2698−2703.
(31) Amundson, K.; Helfand, E.; Quan, X.; Hudson, S. D.; Smith, S. D. Alignment of Lamellar Block Copolymer Microstructure in an Electric Field. 2. Mechanisms of Alignment. *Macromolecules* **1994**, *27*, 6559−6570.
(32) Thurn-Albrecht, T.; DeRouchey, J.; Russel, T. P.; Jaeger, H. M.; et al. Overcoming Interfacial Interactions with Electric Fields. *Science* **2000**, *290*, 3250−3253.
(33) Böker, A.; Knoll, A.; Elbs, H.; Abetz, V.; Müller, A. H. E.; Krausch, G. Large Scale Domain Alignment of a Block Copolymer from Solution Using Electric Fields. *Macromolecules* **2002**, *35*, 1319−1325.
(34) Kyrylyuk, A. V.; Zvelindovsky, A. V.; Sevink, G. J. A.; Fraaije, J. G. E. M. Lamellar Alignment of Diblock Copolymers in an Electric Field. *Macromolecules* **2002**, *35*, 1473−1476.
(35) Tsori, Y.; Andelman, D. Thin Film Diblock Copolymers in Electric Field: Transition from Perpendicular to Parallel Lamellae. *Macromolecules* **2002**, *35*, 5161−5170.
(36) Xu, T.; Hawker, C. J.; Russell, T. P. Interfacial Energy Effects on the Electric Field Alignment of Symmetric Diblock Copolymers. *Macromolecules* **2003**, *36*, 6178−6182.
(37) Xu, T.; Zvelindovsky, A. V.; Sevink, G. J. A.; Lyakhova, K. S.; Jinnai, H.; Russell, T. P. Electric Field Alignment of Asymmetric Diblock Copolymer Thin Films. *Macromolecules* **2005**, *38*, 10788−10798.
(38) Matsen, M. W. Converting the nanodomains of a diblock-copolymer thin film from spheres to cylinders with an external electric field. *J. Chem. Phys.* **2006**, *124*, No. 074906.
(39) Matsen, M. W. Electric Field Alignment in Thin Films of Cylinder-Forming Diblock Copolymer. *Macromolecules* **2006**, *39*, 5512−5520.
(40) Ly, D. Q.; Honda, T.; Kawakatsu, T.; Zvelindovsky, A. V. Hexagonally Perforated Lamella-to-Cylinder Transition in a Diblock Copolymer Thin Film under an Electric Field. *Macromolecules* **2008**, *41*, 4501−4505.
(41) Tsori, Y. Colloquium: Phase transitions in polymers and liquids in electric fields. *Rev. Mod. Phys.* **2009**, *81*, 1471−1494.
(42) Sevink, G. J. A.; Pinna, M.; Langner, K. M.; Zvelindovsky, A. V. Selective disordering of lamella-forming diblock copolymers under an electric field. *Soft Matter* **2011**, *7*, 5161−5170.
(43) Ly, D. Q.; Pinna, M.; Honda, T.; Kawakatsu, T.; Zvelindovsky, A. V. M. Kinetic pathways of sphere-to-cylinder transition in diblock copolymer melt under electric field. *J. Chem. Phys.* **2013**, *138*, No. 074904.
(44) Schoberth, H. G.; Pester, C. W.; Ruppel, M.; Urban, V. S.; Böker, A. Orientation-Dependent Order−Disorder Transition of Block Copolymer Lamellae in Electric Fields. *ACS Macro Lett.* **2013**, *2*, 469−473.
(45) Welling, U.; Müller, M.; Shalev, H.; Tsori, Y. Block Copolymer Ordering in Cylindrical Capacitors. *Macromolecules* **2014**, *47*, 1850−1864.
(46) Dehghan, A.; Schick, M.; Shi, A.-C. Effect of mobile ions on the electric field needed to orient charged diblock copolymer thin films. *J. Chem. Phys.* **2015**, *143*, No. 134902.
(47) Welling, U.; Müller, M. Ordering block copolymers with structured electrodes. *Soft Matter* **2017**, *13*, 486−495.
(48) Pester, C. W.; Liedel, C.; Ruppel, M.; Böker, A. Block copolymers in electric fields. *Prog. Polym. Sci.* **2017**, *64*, 182−214.
(49) Dreyer, O.; Wu, M.-L.; Radjabian, M.; Abetz, C.; Abetz, V. Structure of Nonsolvent-Quenched Block Copolymer Solutions after

https://doi.org/10.1021/acs.macromol.3c01220
Macromolecules 2023, 56, 6880−6890

Exposure to Electric Fields during Solvent Evaporation. *Adv. Mater. Interfaces* **2019**, *6*, No. 1900646.
(50) Daoulas, K. C.; Müller, M. Single chain in mean field simulations: Quasi-instantaneous field approximation and quantitative comparison with Monte Carlo simulations. *J. Chem. Phys.* **2006**, *125*, No. 184904.
(51) Schneider, L.; Müller, M. Multi-Architecture Monte-Carlo (MC) Simulation of Soft Coarse-Grained Polymeric Materials: SOft coarse grained Monte-carlo Acceleration (SOMA). *Comput. Phys. Commun.* **2019**, *235*, 463−476.
(52) Rossky, P. J.; Doll, J.; Friedman, H. Brownian dynamics as smart Monte Carlo simulation. *J. Chem. Phys.* **1978**, *69*, 4628−4633.
(53) Müller, M.; Daoulas, K. C. Single-chain dynamics in a homogeneous melt and a lamellar microphase: A comparison between Smart-Monte-Carlo dynamics, slithering-snake dynamics, and slip-link dynamics. *J. Chem. Phys.* **2008**, *129*, 164906.
(54) Welling, U.; Muller, M.; Shalev, H.; Tsori, Y. Block copolymer ordering in cylindrical capacitors. *Macromolecules* **2014**, *47*, 1850−1864.
(55) Soni, S. S.; Brotons, G.; Bellour, M.; Narayanan, T.; Gibaud, A. Quantitative SAXS Analysis of the P123/Water/Ethanol Ternary Phase Diagram. *J. Phys. Chem. B* **2006**, *110*, 15157−15165.
(56) Hasegawa, H.; Hashimoto, T.; Kawai, H.; Lodge, T. P.; Amis, E. J.; Glinka, C. J.; Han, C. C. SANS and SAXS studies on molecular conformation of a block polymer in microdomain space. *Macromolecules* **1985**, *18*, 67−78.
(57) Harper, C. *Modern Plastics Handbook*; McGraw-Hill, 2000.
(58) Kathrein, C. C.; Kipnusu, W. K.; Kremer, F.; Böker, A. Birefringence Analysis of the Effect of Electric Fields on the Order−Disorder Transition Temperature of Lamellae Forming Block Copolymers. *Macromolecules* **2015**, *48*, 3354−3359.
(59) Blagojevic, N.; Müller, M. Simulation of Membrane Fabrication via Solvent Evaporation and Nonsolvent-Induced Phase Separation. *ACS Appl. Mater. Interfaces* **2023**, DOI: 10.1021/acsami.3c03126.
(60) Milner, S. T.; Morse, D. C. Wetting description of block copolymer thin films. *Phys. Rev. E* **1996**, *54*, 3793−3810.
(61) Tsori, Y.; Andelman, D. Ordering Mechanisms in Confined Diblock Copolymers. *Interface Science* **2003**, *11*, 259−268.
(62) Gunkel, I.; Stepanow, S.; Thurn-Albrecht, T.; Trimper, S. Fluctuation Effects in the Theory of Microphase Separation of Diblock Copolymers in the Presence of an Electric Field. *Macromolecules* **2007**, *40*, 2186−2191.
(63) Schoberth, H. G.; Schmidt, K.; Schindler, K. A.; Böker, A. Shifting the Order-Disorder Transition Temperature of Block Copolymer Systems with Electric Fields. *Macromolecules* **2009**, *42*, 3433−3436.
(64) Orzechowski, K.; Adamczyk, M.; Wolny, A.; Tsori, Y. Shift of the Critical Mixing Temperature in Strong Electric Fields. Theory and Experiment. *J. Phys. Chem. B* **2014**, *118*, 7187−7194.
(65) Tsori, Y.; Tournilhac, F.; Andelman, D.; Leibler, L. Structural Changes in Block Copolymers: Coupling of Electric Field and Mobile Ions. *Phys. Rev. Lett.* **2003**, *90*, 145504.
(66) Xu, T.; Zvelindovsky, A. V.; Sevink, G. J. A.; Gang, O.; Ocko, B.; Zhu, Y.; Gido, S. P.; Russell, T. P. Electric Field Induced Sphere-to-Cylinder Transition in Diblock Copolymer Thin Films. *Macromolecules* **2004**, *37*, 6980−6984.
(67) Wang, J.-Y.; Chen, W.; Russell, T. P. Influence of Interfacial Energy on Electric-Field-Induced Sphere-to-Cylinder Transition in Block Copolymer Thin Films. *Macromolecules* **2008**, *41*, 7227−7231.
(68) Oss-Ronen, L.; Schmidt, J.; Abetz, V.; Radulescu, A.; Cohen, Y.; Talmon, Y. Characterization of Block Copolymer Self-Assembly: From Solution to Nanoporous Membranes. *Macromolecules* **2012**, *45*, 9631−9642.
(69) Marques, D. S.; Vainio, U.; Chaparro, N. M.; Calo, V. M.; Bezahd, A. R.; Pitera, J. W.; Peinemann, K. V.; Nunes, S. P. Self-assembly in casting solutions of block copolymer membranes. *Soft Matter* **2013**, *9*, 5557−5564.
(70) Dorin, R. M.; Phillip, W. A.; Sai, H.; Werner, J.; Elimelech, M.; Wiesner, U. Designing Block Copolymer Architectures for Targeted Membrane Performance. *Polymer* **2014**, *55*, 347−353.

https://doi.org/10.1021/acs.macromol.3c01220
Macromolecules 2023, 56, 6880−6890